ISSN 1027-4510, Journal of Surface Investigation. X-ray, Synchrotron and Neutron Techniques, 2015, Vol. 9, No. 1, pp. 105–110. © Pleiades Publishing, Ltd., 2015.

Rapid Mixing Stopped-Flow Small-Angle X-ray Scattering Study of Lipoplex Formation at Beamline ID02@ESRF[1]

Borislav Angelov[a], Angelina Angelova[b], Markus Drechsler[c], and Sylviane Lesieur[b]

[a] *Institute of Macromolecular Chemistry, Academy of Sciences of the Czech Republic, Heyrovsky Sq. 2, CZ-16206 Prague, Czech Republic*

[b] *CNRS UMR8612 Institut Galien Paris-Sud, Univ Paris Sud 11, F-92296 Châtenay-Malabry, France*

[c] *Laboratory for Soft Matter Electron Microscopy, Bayreuth Institute of Macromolecular Research, University of Bayreuth, D-95440 Bayreuth, Germany*

e-mail: angelov@imc.cas.cz

Received August 14, 2014

Abstract—Rapid mixing stopped-flow experiments, coupled with synchrotron small-angle X-ray scattering (SAXS) on the subsecond timescale, produce a vast amount of experimental structural data. The purpose of this work is to present the key steps of the SAXS data treatment for the case of self-assembly and complexation of cationic lipid particles (vesicles or cubosomes) with plasmid DNA in the course of a rapid mixing stopped-flow process. This approach is significant for the structural analysis of rapidly forming soft-matter biomacromolecular delivery systems.

DOI: 10.1134/S1027451015010279

INTRODUCTION

Small-angle X-ray scattering (SAXS) at high-brilliance beamlines offers the possibility to acquire rapidly single SAXS patterns in a less than a second. This opportunity is essentially important for determination of the structure of liquid crystalline nanoarchitectures incorporating fragile protein, peptide, or nucleic acid molecules that may be damaged by the X-ray beam upon prolonged exposure. In particular, the ID02 beamline at ESRF has been fully dedicated to millisecond time-resolved SAXS experiments [1–5]. Different types of stimulus-triggered kinetic experiments could be performed by SAXS including fast temperature scans [6–10], pressure jumps [11], stopped-flow mixing [12–14] or continuous flow mixing. An example, presented in this study, is the formation of lipoplex nanocarriers (Fig. 1) by assembly of cationic lipid nanoparticles [12, 13, 15–23] and plasmid DNA through stopped-flow mixing.

After completion of the millisecond time-resolved experiments at the synchrotron beamline, the users have to treat a huge amount of raw SAXS data recorded at 4 or 10 ms time resolution. Some procedures, like averaging and calibration, could be done automatically at ID02@ESRF [24]. Nevertheless, the number of experimental data remains colossal, and therefore, the structural analysis and data treatment may take several months (Fig. 2).

[1] The article is published in the original.

The available free software [24, 25] is helpful in some cases, but only a few commercial professional programs have a capacity to treat adequately the sets of hundreds or thousands of frames. In this work, we present results on rapid mixing stopped-flow lipoplex formation with an emphasis on the data treatment of the SAXS pattern sequences by means of a combination of free [24, 25] and commercial [26] software.

EXPERIMENTAL

Materials

Cationic lipid nanoparticles (MO/DOMA/DOPE-PEG_{2000}, 82/15/3 mol %) were prepared by hydration of a lyophilized mixed lipid film as described earlier [3]. The lyophilized mixed film included the nonlamellar monoglyceride lipid 1-oleoyl-rac-glycerol (MO) (M_W = 356.55, purity 99.5%, Sigma), the cationic amphiphile dioctadecyldimethylammonium bromide (DOMA) [27–30] (M_W = 630.95, purity ≥99.0%, Selectophore, Fluka), and the PEGyated lipid 1,2-dioleoyl-sn-glycero-3-phosphoethanolamine-N-(methoxy(polyethylene glycol)-2000) ammonium salt (DOPE–PEG_{2000}) (M_W = 2801.51, purity ≥99.0%, Avanti Polar Lipids). Endotoxin-free plasmid DNA, encoding for human brain-derived neurotrophic factor (BDNF), was prepared by custom gene synthesis, subcloning, and purification (GenScript Co., NJ) using a cloning site of the pEGFP-N1 vector (Clontech).

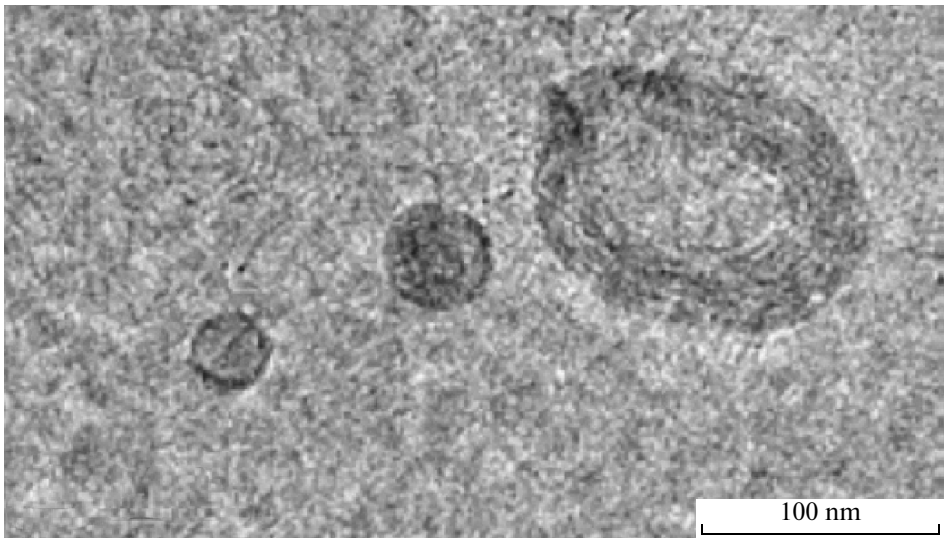

Fig. 1. Cryo-TEM image of lipoplex (MO/DOMA/DOPE-PEG_{2000}/pDNA) nanocarriers generated under equilibrium conditions of mixing of cationic lipid nanoparticles and DNA plasmids. The image is produced from Zeiss EM922 Omega energy-filtered TEM instrument.

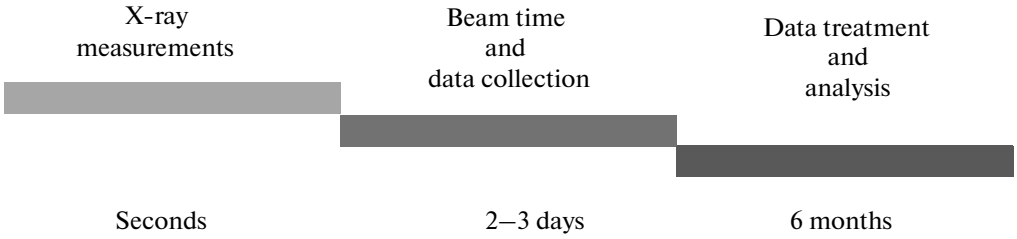

Fig. 2. Time scale from a single measurement at the synchrotron beamline to the final result of the SAXS data analysis.

Synchrotron Radiation Small-Angle X-ray Scattering Coupled with a Rapid-Mixing Stopped-Flow Device

SAXS experiments were performed at the ID02 beamline [2] of the European Synchrotron Radiation Facility (ESRF, Grenoble, France). The time-resolved 2D SAXS patterns were recorded using a high-sensitivity CCD detector (FReLoN 4M) having an active area of 100 × 100 mm which was divided into 512 × 512 pixels with 4 × 4 binning. The X-ray wavelength and sample-to-detector distance were 0.1 nm and 1.5 m respectively, corresponding to an accessible q-range from 0.07 to 3.2 nm^{-1}. The data acquisition sequence was hardware triggered by the stopped-flow device (Fig. 3). Each SAXS pattern was collected over 4, 10 or 100 ms exposure times. Thus, the radiation damage, that could have been a serious problem in the case of continuous exposure to the X-ray beam (4.7×10^{13} photons/s), was avoided. The readout time of the CCD detector was about 190 ms. The normalized 2D patterns were azimuthally averaged automatically to obtain the 1D scattering curves.

Mixing of equal volumes (100 μL) of supercoiled pDNA and PEGylated cationic lipid nanoparticles was performed by a stopped-flow apparatus SFM-400 (Bio-Logic, Claix, France). The scattering cell was fabricated from a quartz capillary (1.5 mm diameter, wall thickness 10 μm) and connected to the outlet of the last mixer [3]. The flow time used for rapid mixing of the two components was 50 ms, during which the kinetic time was equal to the dead time of the stopped-flow device (~2.5 ms). Steady-state SAXS patterns were recorded using a flow-through capillary cell with data acquisition time of 100 ms.

RESULTS AND DISCUSSION

Converting Instrumental Raw SPEC Data into a Common 3D Format

The protocol for SAXS results treatment, proposed here, is organized in key steps (table) that specify the complexity of the treatment of the SAXS data recorded in rapid-mixing stopped-flow structural experiments. The initial phase of these experiments involved loading of lipid nanoparticle dispersions and pDNA solutions [17, 22, 27–36] in the syringes of the stopped-flow apparatus. The volume of the samples and the speed of injection were given as input parameters in the program that controlled the Bio-Logic SFM instrument (Fig. 3). The SAXS measurements were performed by a special command that was

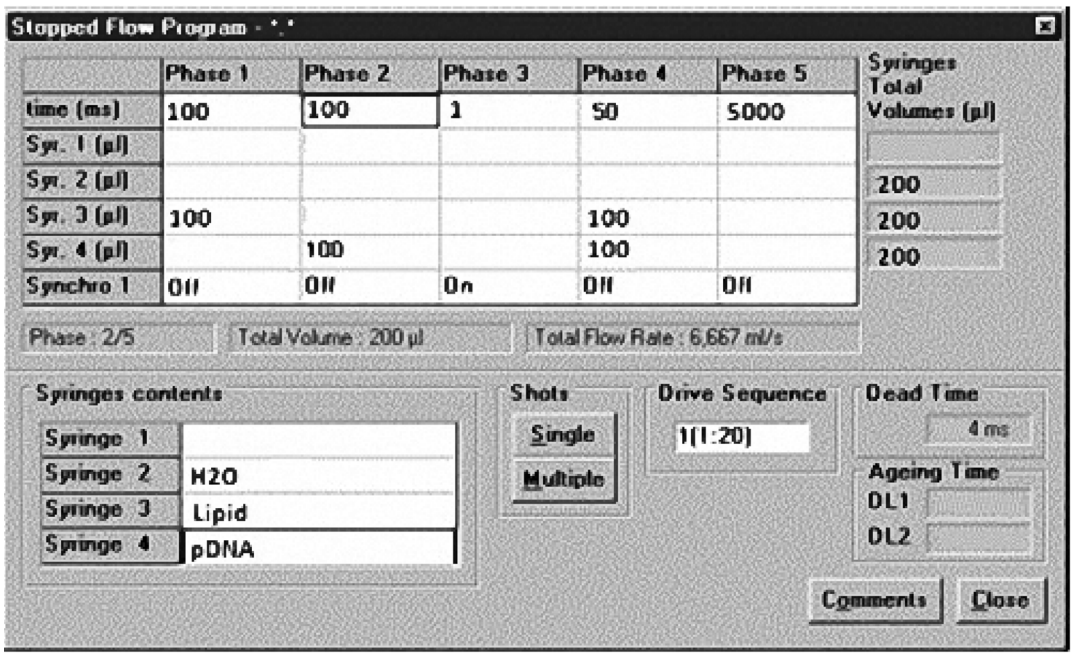

Fig. 3. Example of a control program for stopped-flow mixing of reactants.

entered at the main computer control. The Fig. 4 depicts the command that was employed in our case.

After accomplishment of the command, the measurements were saved in a special data format (SPEC). These data had to be converted into a readable, user-friendly format such as ASCII. This was done via the free software SAXSutilities [24] that is especially developed for the ID02 beamline. Due to internal memory limitations of this program, only 200 frames could be converted at once. Thus, thousands of SAXS patterns were converted into the ASCII format through multiple operations of each 200 frames. Even though, this is a very hardware specific step, similar types of user dependence on the local software can be found at other beamlines producing huge amount of data. The motivation to avoid the user dependence on SAXSutilities arises also from the differences in the particular versions or updates of this software.

The next step of the data treatment required the subtraction of the background associated with the

Sequence of the steps involved in the collection and treatment of large volume of millisecond time-resolved SAXS data

Step	Description
1	Executing a command for millisecond time-resolved rapid-mixing stopped-flow measurement. An example is presented in the Fig. 4
2	Using the SAXSUtillities software to export every SPEC frame to an ASCII format
3	Repetition of step 2 several times in groups of 200 frames
4	Using the Mathematica for subtraction of the background from every frame. Calibration of the data by dividing the intensity over the capillary thickness
5	Calculation of the millisecond time, t, corresponding to every measured SAXS pattern in the performed rapid-mixing stopped-flow shots
6	Grouping the data of all stopped-flow shots in one Math file. Prepending the SAXS pattern at time zero using the sum of the initial static states (i.e. lipid nanoparticles and pDNA). Adding the last static frame at the end of the stop-flow cycle
7	Plotting the SAXS patterns as 3D frames
8	Selection and plotting of around 150 representative frames in order to reduce the size of the Math file
9	Selection of 10 key patterns for fitting analysis. Exporting of the data in a CSV format
10	Indexing of the diffraction peaks, if any
11	Fitting of the SAXS data with a model (SASFit) in order to determine the precise liquid crystalline nanostructures
12	Plotting of the reaction kinetics curve, which describes the structural pathway of the nanoparticles assembly with pDNA

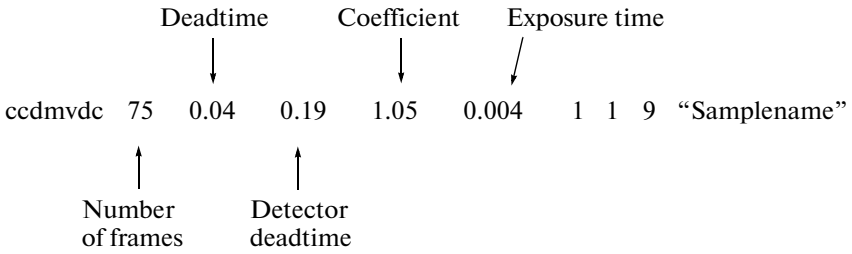

Fig. 4. Command for SAXS data collection in rapid-mixing stopped-flow experiments at ID02 beamline of ESRF. The times are indicated in seconds.

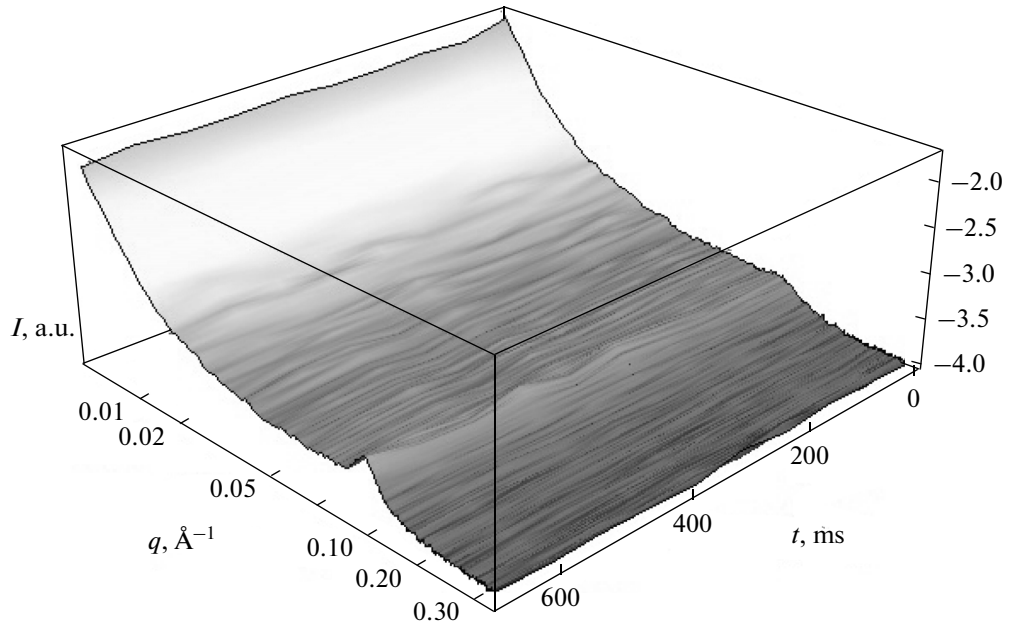

Fig. 5. 3D plot of millisecond time-resolved SAXS patterns produced in step 7 of the data analysis (table). The axes are on a logarithmic scale.

stopped-flow sample holder tube (filled with ultrapure water), followed by division of the outcome by the tube thickness (which is typically 1.5 mm). Multiple frames (20–30) from the measured scattering background of the quartz capillary and the solvent (i.e. water) were averaged using the SAXSUtilities and converted to ASCII format. The subtraction of the different sets of data and the thickness calibration can be done via different software programs such as Matlab, Mathematica or Origin. We employed Mathematica [26] in our data analysis. All next steps were performed with the help of this program.

A specific feature of the detector at the ID02 beamline was that it had a relatively long data transfer time of ~190 ms. The methodology for collection of SAXS patterns at shorter times consisted in performing several stopped-flow rapid mixing shots with new sample injections. Practically, the experiment was repeated many times with a variable initial input delay time for the first SAXS pattern measurement. The number of rapid-mixing shots to be performed was unknown in advance. It was dependent on the available sample volume and the user's aims. We performed data collection during nine shots for every reactant concentration. This permitted us to determine and register all key events of the kinetic pathway during the first 190 ms. The next step of the data treatment comprised the calculation of the time (t) at which every SAXS frame was measured. This was followed by subsequent sorting of the frames according to their times of acquisition, $t > t_0$. The calculation of the time t involved six time constants related to the detector deadtime (190 ms), exposure time (4 ms), stopped flow deadtime (~2 ms), stopped flow mixing time (50 ms), frame shift time, and frame number time.

The time-sorted frames were appended with the zero-time frame (recorded at t_0 as a sum of the initial intensities of the solution components, i.e. of the lipid nanoparticles and of the DNA plasmids). The last

frame of the recorded rapid-mixing shots ($t = t_\infty$) was also included in the data ensemble. It corresponded to the final state of the self-assembled system achieved under equilibrium conditions [22]. The step 6 yielded a file in Mathematica format, which included all SAXS patterns of the performed stopped-flow rapid-mixing shots arranged according to the time of their acquisition. An advantage of using Mathematica for data analysis is that it may produce 3D plots of the SAXS patterns (Fig. 5).

Identification of the SAXS Frames Representing Distinct Structural Models

The 3D plotting indicated whether all recorded SAXS frames contained unique structural information or a fraction of them could be discarded from the analysis because of coincidence (step 8 and Fig. 6a). Visual inspections of the obtained 3D plots revealed the qualitative behaviour of the lipid nanoparticulate system subjected to self-assembly and complexation with biomacromolecules (pDNA). Nanoparticle-nanoparticle structural transitions from one mesophase organization to another one (for instance a lamellar–to–nonlamellar transition) were possible. To establish this fact, the data were saved for a further detailed analysis in the CSV format (step 9) and fitted with a free software programs such as SASFit [25].

Some of the lipid nanoparticulate carriers exhibited internal structural order (Fig. 6b). In this case, the following step (step 10) required indexing of the observed peaks and identification of the crystallographic space group of the liquid crystalline nanostructures. Fitting models are available for bicontinuous lipid cubic structures [35, 36]. They may be employed for determination of the bilayer thickness of the cubic membranes that built-up the lipid nanocarriers (step 11).

The increasing Bragg peak at $q \approx 0.125$ Å^{-1} (d-spacing, $d \approx 5$ nm) in the SAXS pattern shown in the Fig. 6a gave an evidence for the formation of an onion internal structure in the lipid particles after pDNA upload. A second Bragg peak did not appear, thus indicating the impossibility for the pDNA molecules to arrange into a well-defined lattice. The d-spacing value ~5 nm suggested a confinement of the supercoiled pDNA in nanoparticles of weakly ordered bilayer structures. After an initial exponential growth, the Bragg peak intensity reached a steady-state level after approximately 95 ms.

In a final step, a kinetic graph of the reaction pathways was constructed based on calculations of the areas under the scattering $I(q)$ curves (Fig. 6c). The model of random sequential absorption kinetics [37–39] was best applicable to the kinetics of the investigated lipoplex formation. The obtained kinetic curve was fitted in order to determine the time constant of the complexation between the cationic lipid membranes and pDNA in the nanocarriers. This kinetics, elucidated on the time scale of milliseconds, corresponds to the formation of intermediates, in which the secondary structure of pDNA becomes more compact.

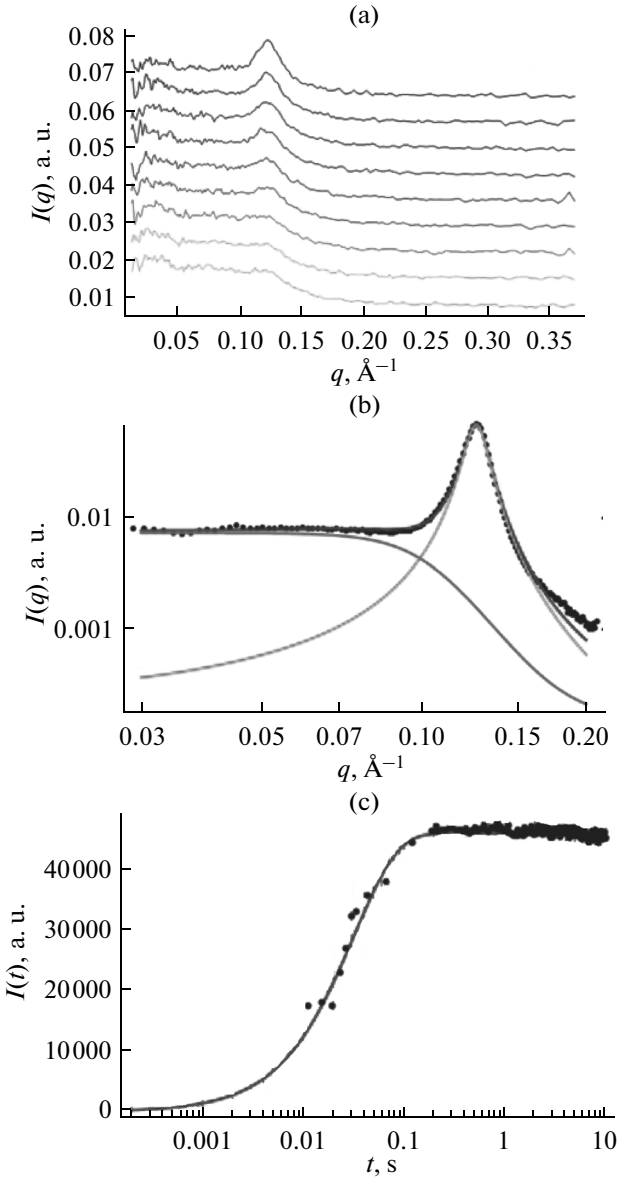

Fig. 6. Selection of representative SAXS frames (a), model fitting of the scattering peak characterizing the inner structural organization of the lipoplex particles (b), and a kinetic curve intensity versus time (c).

CONCLUSIONS

The described experimental procedure represents a useful systematic way to treat large ensembles of millisecond time-resolved structural SAXS data. It can be

applied to evaluate the fast occurring structural kinetic pathways of assembly of other types of nanoparticles and biomacromolecules based on time-resolved SAXS experiments.

ACKNOWLEDGMENTS

The ESRF (European Synchrotron Radiation Facility, Grenoble, France) is thanked for granting SAXS beam time (project SC-3358 at the ID02 beamline) and Drs. T. Narayanan, S. Filippov and P. Stepanek for their kind help, collaboration and support. This work was supported by Czech Science Foundation (Grant no. P208/10/1600), ANR SIMI10 Nanosciences, LabEx LERMIT, BIMF (Bayreuth Institute of Macromolecular Research), and BZKG (Bayreuth Center for Colloids and Interfaces).

REFERENCES

1. P. Panine, S. Finet, T. M. Weiss, and T. Narayanan, Adv. J. Colloid Interface Sci. **127**, 9 (2006).
2. T. Narayanan, Curr. Opin. J. Colloid Interface Sci. **14**, 409 (2009).
3. B. Angelov, A. Angelova, S. K. Filippov, T. Narayanan, M. Drechsler, P. Štěpánek, P. Couvreur, and S. Lesieur, J. Phys. Chem. Lett. **4**, 1959 (2013).
4. P. Saveyn, P. van der Meeren, M. Zackrisson, T. Narayanan, and U. Olsson, Subgel Soft Matter **5**, 1735 (2009).
5. R. Lund, L. Willner, D. Richter, P. Lindner, and T. Narayanan, ACS Macro Lett. **2**, 1082 (2013).
6. A. Angelova, B. Angelov, B. Papahadjopoulos-Sternberg, M. Ollivon, and C. Bourgaux, J. Drug Deliv. Sci. Technol. **15**, 108 (2005).
7. A. Angelova, B. Angelov, S. Lesieur, R. Mutafchieva, M. Ollivon, C. Bourgaux, R. Willumeit, and P. Couvreur, J. Drug Deliv. Sci. Technol. **18**, 41 (2008).
8. A. Yaghmur and M. Rappolt, Eur. Biophys. J. **41**, 831 (2012).
9. Y.-D. Dong, A. J. Tilley, I. Larson, M. J. Lawrance, H. Amenitsch, M. Rappolt, T. Hanley, and B. J. Boyd, Langmuir **26**, 9000 (2010).
10. A. Angelova, B. Angelov, V. M. Garamus, P. Couvreur, and S. J. Lesieur, Chem. Phys. Lett. **3**, 445 (2012).
11. C. E. Conn, O. Ces, X. Mulet, S. Finet, R. Winter, J. M. Seddon, and R. H. Templer, Phys. Rev. Lett. **96**, 108102 (2006).
12. P. C. Barreleiro and B. Lindman, J. Phys. Chem. B **107**, 6208 (2003).
13. P. C. A. Barreleiro, R. P. May, and B. Lindman, Faraday Discuss. **122**, 191 (2002).
14. A. Yaghmur, P. Laggner, B. Sartori, and M. Rappolt, PloS ONE **3**, 2072 (2008).
15. J. J. Wheeler, L. Palmer, M. Ossanlou, I. MacLachlan, R. W. Graham, Y. P. Zhang, M. J. Hope, P. Scherrer, and P. R. Cullis, Gene Therapy **6**, 271 (1999).
16. G. Tresset and Y. Lansac, J. Phys. Chem. Lett. **2**, 41 (2011).
17. T. A. Balbino, A. A. M. Gasperini, C. L. P. Oliveira, A. R. Azzoni, L. P. Cavalcanti, and L. G. de la Torre, Langmuir **28**, 11535 (2012).
18. J. Gustafsson, G. Arvidson, G. Karlsson, and M. Almgren, Biochim. Biophys. Acta **1235**, 305 (1995).
19. G. Caracciolo, D. Pozzi, R. Caminiti, C. Marchini, M. Montani, A. Amici, and H. Amenitsch, J. Phys. Chem. B **112**, 11298 (2008).
20. Y. S. Tarahovsky, Biochemistry (Moscow) **74**, 1293 (2009).
21. M. B. Bally, Y.-P. Zhang, F. M. P. Wong, S. Kong, E. Wasan, and D. L. Reimer, Adv. Drug Deliv. Rev. **24**, 275 (1997).
22. B. Angelov, A. Angelova, S. Filippov, G. Karlsson, N. Terrill, S. Lesieur, and P. Štěpánek, Soft Matter **7**, 9714 (2011).
23. A. Massotti, G. Mossa, C. Cametti, G. Orgaggi, A. Bianco, N. del Grosso, D. Malizia, and C. Esposito, Colloids Surf. B **68**, 136 (2009).
24. SAXS Utilities software. www.sztucki.de/SAXSutilities/
25. SASFit software. kur.web.psi.ch/sans1/SANSSoft/sasfit.html
26. Wolfram Mathematica 9.0. www.wolfram.com/mathematica/
27. J. G. Petrov and A. Angelova, Langmuir **8**, 3109 (1992).
28. A. Angelova, J. G. Petrov, T. Dudev, and B. Galabov, Colloids Surf. **60**, 351 (1991).
29. J. G. Petrov, D. M. Moebius, and A. Angelova, Langmuir **8**, 201 (1992).
30. J. G. Petrov, A. Angelova, and D. Moebius, Langmuir **8**, 206 (1992).
31. B. Angelov, A. Angelova, B. Papahadjopoulos-Sternberg, S. V. Hoffmann, V. Nicolas, and S. Lesieur, J. Phys. Chem. B **116**, 7676 (2012).
32. B. Angelov, A. Angelova, B. Papahadjopoulos-Sternberg, S. Lesieur, J.-F. Sadoc, M. Ollivon, and P. Couvreur, J. Am. Chem. Soc. **128**, 5813 (2006).
33. A. Angelova, B. Angelov, M. Drechsler, V. M. Garamus, and S. Lesieur, Protein Int. J. Pharm. **454**, 625 (2013).
34. D. McLoughlin, M. Imperor-Clerc, and D. Langevin, Chem. Phys. Chem. **5**, 1619 (2004).
35. B. Angelov, A. Angelova, V. M. Garamus, M. Drechsler, R. Willumeit, R. Mutafchieva, P. Štěpánek, and S. Lesieur, Langmuir **28**, 16647 (2012).
36. M. Nakano, T. Teshigawara, A. Sugita, W. Leesajakul, A. Taniguchi, T. Kamo, H. Matsuoka, and T. Handa, Langmuir **18**, 9283 (2002).
37. E. Maltsev, J. Wattis, and H. Byrne, Phys. Rev. E **74**, 011904 (2006).
38. A. Angelova, B. Angelov, M. Drechsler, and S. Lesieur, Drug Discov. Today **18**, 1263 (2013).
39. Z. Almshergi, S. Hyde, M. Ramachandran, and Y. Deng, J. R. Soc. Interface **5**, 1023 (2008).